Journal of Atmospheric and Solar-Terrestrial Physics 185 (2019) 7–21

Contents lists available at ScienceDirect

Journal of Atmospheric and Solar-Terrestrial Physics

journal homepage: www.elsevier.com/locate/jastp

Application of the T2-Hotelling test for investigating ionospheric anomalies before large earthquakes

Zahra Sadeghi, Masoud Mashhadi-Hossainali*

Department of Geodesy and Geomatics Engineering, K. N. Toosi University of Technology, No. 1346, Vali_Asr Ave., Mirdammad Cr., Tehran, Iran

ARTICLE INFO

Keywords:
Earthquake
Ionospheric anomalies
TEC
T2-hotelling test

ABSTRACT

In view of the frequent occurrence of large earthquakes, researchers have been always looking for ways to study and analyze these risky phenomena. Today, abnormal changes in ionosphere are taken as a means for this purpose. This article concentrates on the application of the T2-Hotelling test for detecting significant changes in the Total Electron Content (TEC) as an ionospheric parameter. The Global Ionosphere Maps (GIMs) are used for this purpose. The basic assumption is that TECs are normally distributed. This has been analyzed by using ten normality tests. Proposed method statistically analyzes the mean TEC changes using two samples of TECs. The first or the reference sample is 30 days long. The second or the target sample which is a moving one in time is 4 days long. The method is applied to the entire globe and therefore is a global method in nature. TECs associated with high solar and/or geomagnetic activity are not used when the reference sample is made. A sample of 12 earthquakes, occurred in 2010, with the moment magnitudes greater than 6 is used to analyze the efficiency of the proposed method. For 75% of the earthquakes in this study, proposed method confirms the seismo-ionospheric anomalies some of which have been already reported in the other researches. The rest of the studied quakes conform to the assertion that seismo-ionospheric anomalies might not be clearly visible even for some large earthquakes.

1. Introduction

Earthquake is one of the most destructive and damaging natural disaster. On average, annually an earthquake with the magnitude of M≥ 8.0 and fifteen with the magnitude of M≥ 7.0 occur in the world (Le et al., 2015). This leads to huge losses of life and property to the people all around the world. Earthquake is a seismic geophysical phenomenon including irregular, nonlinear and complex processes and that's why there is no simple approach to predict its parameters (Akhoondzadeh and Saradjian, 2011), notwithstanding the fact that seismic activities of the Earth are effective on ionospheric parameters. Researchers have reported abnormal ionosphere changes prior to large earthquake (seismo-ionospheric anomalies). Alaska earthquake with the magnitude of Mw = 9.3 and depth of 25 km, occurred on 28 March 1964, was the first earthquake whose ionospheric changes were considered (Davies and Baker, 1965; Leonard and Barnes, 1965). Following that, in many studies the variations of ionospheric parameters have been discussed for large earthquakes. The TEC data survey had a significant role in discovery of seismo-ionospheric anomalies. Liu et al. (2001) used the TEC obtained from GPS observations to study the ionospheric changes in the Chi-Chi earthquake with the magnitude and depth of Mw = 7.7 and d = 33 km, respectively. According to that study, TEC is considerably reduced around the earthquake epicenter, one, three and four days before it takes place (Liu et al., 2001). By investigating the TEC parameters derived from a local tracking network, Liu et al. (2004) show that for 16 out of 20 earthquakes with the magnitude of M≥ 6 and depth range of 1.7–280.4 km, TEC is substantially reduced in the afternoon or evening of 1–5 days before the earthquake (Liu et al., 2004). Subsequent to that research, other studies represented an unusual increase or decrease in TEC before large earthquakes. Such anomalies are either seen in an area near the epicenter of the earthquake or sometimes in the corresponding geomagnetic conjugate region (Ho et al., 2013; Liu et al., 2009; Liu et al., 2011b; Su et al., 2013; Ulukavak and Yalcinkaya, 2016; Xu et al., 2011; Zhao et al., 2008; Zhu et al., 2014). Le et al. (2011) examined a sample of 736 earthquakes with magnitude of M≥ 6 and the depth range of not less than 40 km. To investigate the ionospheric anomalies, the CODE TEC maps were used in that research. They concluded that the incidence rate of anomaly a few days before a large earthquake was higher than the other days and more anomalies could be observed for earthquakes with higher magnitude and lower depth (Le et al., 2011). Employing the GIMs Yao et al. (2012a,b) asserted seismo-ionospheric features that were previously

* Corresponding author.
E-mail addresses: z.sadeghi@mail.kntu.ac.ir (Z. Sadeghi), hossainali@kntu.ac.ir (M. Mashhadi-Hossainali).

https://doi.org/10.1016/j.jastp.2019.01.010
Received 13 July 2018; Received in revised form 19 January 2019; Accepted 21 January 2019
Available online 01 February 2019
1364-6826/

reported for ionospheric anomalies. They also reported on some observed features such as: anomaly occurs frequently in the region near the epicenter, however they observed that the maximum affected area in the ionosphere does not coincide with the vertical projection of the epicenter of the subsequent earthquake and the direction of this deviation does not follow a fixed rule. On the other hand, sometimes these anomalies can also be seen in the geomagnetic conjugate region, but the extent and probability of this is relatively less than the area near the epicenter (Yao et al., 2012b).

The background mechanism has been explained in terms of geochemical and geophysical processes such as: the electric fields that are produced by the compression of rocks near the center of an earthquake (Parrot, 2017), unstable thermal anomalies generated by warm gasses emanated through the rising fluids under the ground (Hayakawa and Molchanov, 2002), earthquake-related electrical signals and EM emissions due to rapid movements or fluctuating charge clouds produced through the activation of positive holes and their attendant sound waves (Freund, 2002), and emissions of radioactive gas or metallic ions, such as radon, which leads to increasing potential at the Earth's surface (Harrison et al., 2010; Pulinets et al., 2003). In a nutshell, Acoustic Gravity Waves (AGW) produced by the Earth's crustal movements, thermal anomalies and the dispersion of lithospheric gasses into the atmosphere is one of the most accepted mechanisms in this respect (Calais and Minster, 1995; Liperovsky et al., 2008; Liu et al., 2008; Pertsev and Shalimov, 1996; Shalimov and Gokhberg, 1998; Zhao and Hao, 2015). Dispersion of radioactive gasses together with the other influencing parameters increase the electric potential and thereby the electric conductance of the atmosphere near to the surface of the Earth. These changes impacts the electric field of the E layer. Penetration of the perturbed electric field into the ionosphere changes the electron density there (Le et al., 2015).

Anomaly detector methods are usually based on the analysis of the spatio-temporal variation of an ionospheric parameter. To this end, a reference value; either the mean or median which is derived from a sample of 15–30 days length (reference sample), is derived for the desired parameter. The detection process is generally based on the comparison of the parameter values to the reference one. In case observed anomalies can be interrelated to the location and the occurrence time of an earthquake, the observed anomalies are regarded as sismo-ionopheric ones (Akhoondzadeh, 2013e; Li et al., 2016; Liu et al., 2000, 2006, 2009; Su et al., 2013; Zhu et al., 2014). Application of the classical and intelligent methods including Kalman filter, Artificial Neural Network (ANN), Paticle Swarm Optimization (PSO), Auto-Regressive Integrated (ARIMA), Fuzzy Logic (FL), Support vector machine (SVM) and Genetic Algoritm (GA) have revealed strong potentials in time series prediction, but time consuming dependce on linearity and size of data (especially when the data is in global scale), complexity and non-unique solution are numerated as some of their disadvantages (Akhoondzadeh, 2011, 2012, 2013a, b, c, e, 2014; Hirooka et al., 2011; Jyh-Woei, 2011; Lognonné et al., 2006).

Here, the anomaly detector method is based on the application of the univariate T2-Hotelling test to GIMs (as a global scale data) and the accepted characteristics for seismo-ionospheric anomalies. Through this, detected variations in the TEC are assigned to certain earthquakes. A sample of 12 large earthquakes distributed worldwide is used for this purpose. The analysis start 15 days before every earthquake and it is applied to all of the GIMs' nodes. This implies that the method is applied 735840 times to the input data for each of the studied quakes. The T2-Hotelling tests together with the adopted methodology for its application are given in the next section of this paper. The data and the studied earthquakes are described then in the third section of this research. Finally, the implementation of results for every earthquake are presented and discussed, separately.

2. Univariate two-sample T2-Hotelling test

T2-Hotelling test was first discussed in 1931 by Harold Hotelling at a meeting of the Mathematical Association of America (Hotelling, 1992). This is a statistical test which examines the difference between the mean of two samples. The method, which is the same as the Likelihood Ratio Test, remains unchanged if the observation unit changes. Also, among all unbiased tests (tests whose power for all values of the parameter is greater than or equal to the level of significance), the T2-Hotelling is uniformly of the highest power (Srivastava and Carter, 1983).

Assuming that $x_{11}, x_{12}, \ldots, x_{1N_1}$ and $x_{21}, x_{22}, \ldots, x_{2N_2}$ are independent normally distributed samples with parameters μ_1, μ_2 and σ^2 , i.e. $N(\mu_1, \sigma^2)$ and $N(\mu_2, \sigma^2)$, the univariate two-sample T2-Hotelling test analyzes the null hypothesis H_0: $\bar{\mu}_1 = \bar{\mu}_2$ against the alternative one, H_1: $\bar{\mu}_1 \neq \bar{\mu}_2$. To perform this test the mean ($\bar{x}_i$) and standard deviation (S_i) of each sample is calculated using the following formula:

$$\bar{x}_i = \frac{1}{N_i}\sum_{j=1}^{N_i} x_{ij} \qquad i = 1,2 \tag{1}$$

$$S_i^2 = \frac{1}{n_i}\sum_{j=1}^{N_i} (x_{ij} - \bar{x}_i)^2 \;\; i = 1,2 \tag{2}$$

In these equations, N_i is the sample size and $n_i = N_i - 1$. The pooled variance is then computed by:

$$S_p^2 = \frac{n_1 S_1^2 + n_2 S_2^2}{f} \tag{3}$$

Where $f = n_1 + n_2 = N_1 + N_2 - 2$ is known as the degree of freedom. The null hypothesis is rejected if and only if (Srivastava and Carter, 1983):

$$\left(\frac{N_1 N_2}{N_1 + N_2}\right)^{1/2} \left|\frac{\bar{x}_1 - \bar{x}_2}{S_p}\right| > t_{f,\alpha/2} \tag{4}$$

Or:

$$\left[\left(\frac{N_1 N_2}{N_1 + N_2}\right)\frac{(\bar{x}_1 - \bar{x}_2)^2}{S_p^2}\right] > t_{f,\alpha/2}^2 \equiv F_{1,f,\alpha} \tag{5}$$

Here, $t_{f,\alpha/2}$ is the critical value derived from the Student's t-distribution, α is the significant level and $F_{1,f,\alpha}$ is the critical value derived from the Fisher distribution. The basic assumption for T2-Hotelling test is that the distribution of data must be normal.

In this study, the T2-Hotelling test is conducted at the confidence levels of 99% and 95%. The critical value increases by increasing the confidence level, if the samples' sizes are held fixed. To reject the test at a higher confidence level, the difference of the means should therefore increase. In other words, the intensity of anomalies detected is higher at the confidence level of 99% but, the anomalies are detected more frequently when the confidence level is 0.95.

In order to analyze the TEC anomalies, here the closest grid point of GIMs to the earthquake epicenter (test point) is firstly taken into account. The CODE GIM products for a time period of 45 days including 44 days before and the day of the earthquake are used for this purpose. The first or the reference sample is constructed by stacking the values of TEC at the test point. This is done for every 2 h epochs, i.e. 0 h, 2 h, 4 h, …and 12 h.

The second or the target sample is constructed using the remaining 15 days (14 days before and the day of earthquake) in the form of four-day intervals such that in the first step, it covers the 14th, 13th, 12th and 11th days before the earthquake. Each time the hypothesis test is run, the time period of the second sample is moved one day ahead. To be more specific, when the test is run for the second time, the new

sample is constructed by stacking the daily values of TEC at 13th, 12th, 11th and 10th days before the earthquake. Following this procedure, for the last run of the test; the second sample includes the daily values of TEC at 3rd, 2nd, 1st day before and the day of earthquake. Thus, the target sample is a moving sample in time. Next, the test is run for the other grid nodes. Based on the above discussion, the T2-Hotelling test is repeated 144 times for every grid points of the GIMs. Each time the TEC anomaly is analyzed, using a single sample group (the reference and one of the target samples). The rejection of the null hypothesis confirms that a remarkable difference exists between the mean TECs derived from the reference and the corresponding target samples. Once a significant variation is confirmed by this hypothesis test, using the same method, variation of TEC is analyzed at the other grid points. This provides an insight into the spatial distribution of TEC anomaly during the time period of interest.

3. Earthquakes and input data

The time resolution of the applied GIMs is 2 h. Such maps model the VTEC in a solar-geomagnetic reference frame. GIMs cover the latitudes range of $+87.5^{\circ}$ to -87.5° and the longitudes range of $+180^{\circ}$ to -180°. The spatial resolution of these models is 2.5° in latitude and 5° in longitude. They are available to users at UNIBE (ftp://ftp.unibe.ch/aiub/CODE). In this study, the geomagnetic indices of *Kp* and *Dst* , also the solar radio flux index $F10.7$ are used as the required measures for filtering the input data. Indices of *Kp* and $F10.7$ are available through SPIDR[1] and the *Dst* index is available through ISGI.[2] To be more specific, days at which $Kp \geq 4$ and/or $Dst \leq -40$ are not taken into account. This study concentrates on the year 2010 because, solar activity is low in this period of time. Moreover, the following criteria are used for selecting the earthquakes:

1) The approximate radius of the area affected by an earthquake is given by $R = 10^{0.43M}$ where R is the radius in km and M is the moment magnitude, respectively. This area is also known as the affective preparation zone (Dobrovolsky et al., 1979). Considering the grid size of GIMs (278 by 556 km), seismo-ionospheric anomalies of earthquakes with the moment magnitude of 6 or more are expected to be identified by such models. This criterion is also used in (Le et al., 2011; Liu et al., 2009, 2010; Yao et al., 2012b; Zhu et al., 2014).
2) Selected earthquakes are located in different latitudes.
3) The magnitude of the other earthquakes located in the area defined by R is smaller than $M_w = 6$.
4) GIMs are more reliable where the distribution of the Ionospheric Pierce Point (IPPs) is large. Therefore, earthquakes located in such areas are taken into account.

Based on these criteria, 12 earthquakes have been selected for this research. The spatial distributions of these earthquakes together with their faulting mechanism are given in Fig. 1. The focal mechanism and other information of the given quakes are based on the CMT[3] and USGS[4] data bases. Table 1 also provides an overview on the magnitude and depth of these earthquakes. Although the above criteria reduces the sample size of this study especially when it is compared to researches such as (Le et al., 2011), but it benefits from the clear advantage that the problem is analyzed within the entire globe. Therefore, from the point of view of the mathematical statistics; the adopted sample is not small. Moreover, earthquake is a seismic geophysical phenomenon including irregular, nonlinear and complex processes and that's why there is no simple approach to predict its parameters (Akhoondzadeh and Saradjian, 2011). Simplifying the analysis of such a process is obviously inevitable specially when a single parameter (the TEC variation in this study for example) is used for this purpose. The applied criterions are obviously supportive in this respect.

4. Numerical results and discussion

As explained in part 2, the basic assumption for the T2-Hotelling test is that the distribution of data must be normal. To investigate this, ten well-known normality tests (Kolmogorov-Smirnov in Limiting form (KS-Lim), Stephens Method (KS−S), Marsaglia Method (KS-M), Lilliefors (KS-L), Anderson-Darling (AD), Cramer-Von Mises (CvM), Shapiro-Wilk (SW), Shapiro-Francia (SF), Jarque-Bera (JB) and DAgostino and Pearson (DAP) tests) are used. The tests are applied to the input data in every 2 h epochs, (i.e. 0 h, 2 h, 4 h, …and 12 h). Results corresponding to the first epoch and the KS-L method is given in Fig. 2. According to the obtained results the T2-Hotelling test can be applied to the TEC data. Points in red illustrate the nodes for which the distribution of TEC is not normal. Such nodes are usually located in the areas where the distribution of the IPPs is low. In this study, we ignore such grid points because; they do not fulfill the basic assumption required in the T2-Hotelling test.

The T2-Hotelling test is firstly applied at the test point of every earthquake. Table 3 and A1 to A11 report on the corresponding results. Superscripts '†' and '††' are used to distinguish the time periods of significant anomalies. They are also used to identify the confidence levels, i.e. 95% and 99% respectively. After that the spatial distribution of the TEC anomalies are studied for every earthquake during the time periods in which significant TEC anomalies are detected in the previous step. This is done for every sample group and within the entire globe, separately. The anomalies that are detected by the T2-Hotelling test are associated to a certain seismic event if the frequency of the observed changes is high, they occur at the effective precursor manifestation zone (and/or the corresponding geomagnetic conjugate region) and they happen in a relevant period of time. These features have been frequently observed when ionospheric changes are analyzed before a large earthquake and therefore they are already regarded as the characteristic features of seismo-ionospheric anomalies associated with large earthquakes. Finally, sample pairs with significant anomalies are distinguished next. These groups are given in bold (see Table 3 and A1 to A11). The spatial distribution of siesmo-ionospheric anomalies are given in Fig. 3 and A1 to A8. In these figures, the time intervals for the anomalies are similar to the related test points. Moreover, grids points at which the RMS error of TECs is larger than the estimated TECs are not considered at all. The magnetic equator and the two bands of enhanced electron densities that lie parallel to the magnetic equator, centered at the geomagnetic latitudes of about $\pm 20^{\circ}$, are also drawn. The earthquake epicenter and its geomagnetic conjugate point are marked with star and triangle, respectively.

Further details concerning the coordinates of the test points, the time periods of analysis, time periods of geomagnetic activities (days with high geomagnetic activity), the degree of freedom, critical values in every T2-Hotelling test and the sample pairs for which a significant seismo-ionospheric anomaly is seen are given in Table 2.

Similar to the other researches (Akhoondzadeh, 2013d; Alcay, 2016; He and Heki, 2016; Li et al., 2016; Liu et al., 2009; Liu et al., 2006; Liu et al., 2000; Liu et al., 2004; Nenovski et al., 2015; Oikonomou et al.; Pulinets and Boyarchuk, 2004; Su et al., 2013; Yao et al., 2012a; Yiyan et al., 2009; Zhu et al., 2013; Zhu et al., 2014) in this study a reference value is used for detecting the TEC anomalies. Here, this value is the mean TEC for the reference sample. The reference value is always dependent on the reference sample. For example, whether the abnormal changes in TECs due to the high solar and/or geomagnetic activity are filtered when the reference sample is made, impacts the estimated reference value. As the result, the comparison of our results to those that

[1] Space Physics Interactive Data Resource (http://spidr.ngdc.noaa.gov/spidr).
[2] International Service of Geomagnetic Indices (http://isgi.unistra.fr).
[3] http://globalcmt.org.
[4] http://earthquake.usgs.gov/earthquakes.

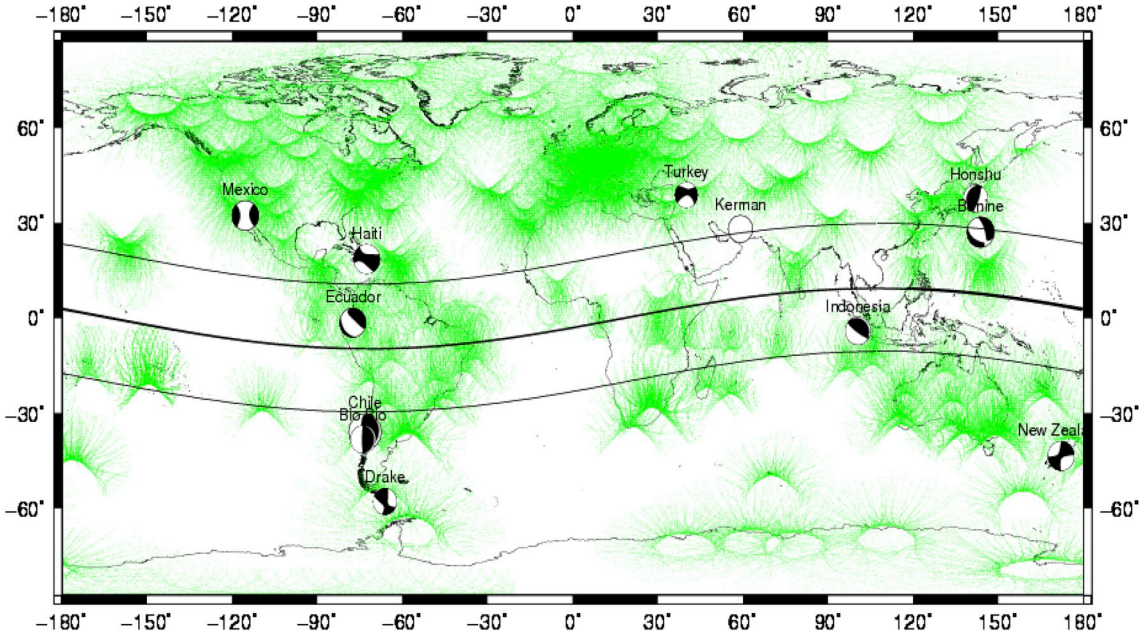

Fig. 1. Distribution of selected earthquakes and the IPP positions. Beach balls illustrate the focal mechanism of each quake.

Table 1
Magnitude and depth of selected earthquakes.

Earthquake	Haiti	Drake Passage	Chile	Indonesia	Turkey	Honshu	Mexico	Bio-Bio	Ecuador	New Zealand	Kerman	Bonin
Magnitude (Mw)	7.0	6.3	8.8	6.8	6.1	6.5	7.2	6.6	7.1	7.0	6.7	7.4
(km)Depth	13	5	22.9	26	12	32	10	22	206.7	12	12	14

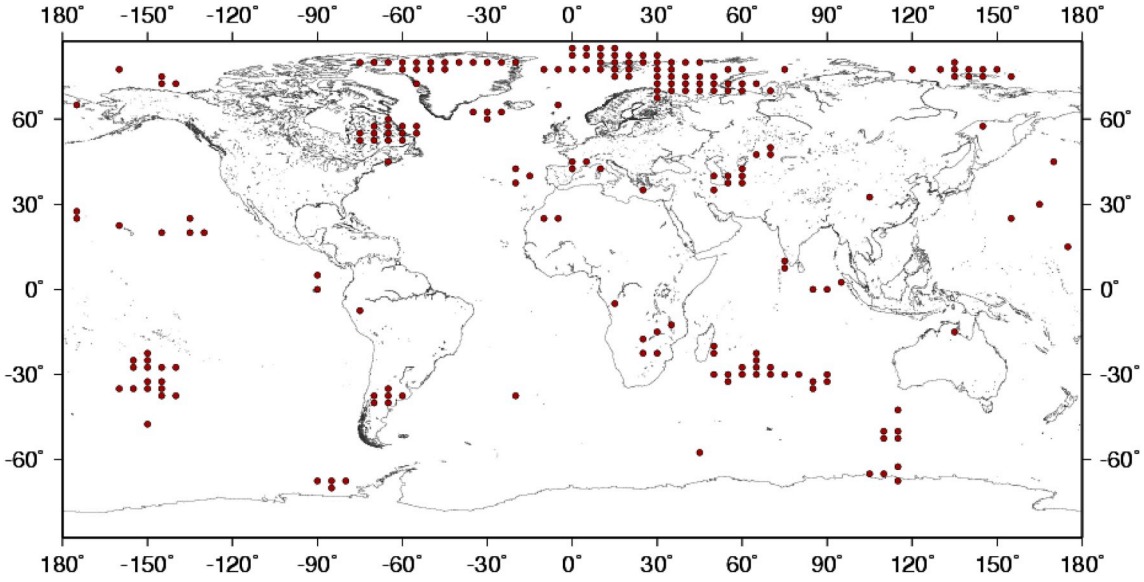

Fig. 2. Result of the Lilliefors test for the first epoch. Points are rejected in the test.

Table 2
A brief overview on the input data of this research. TEC data for the time periods given in bold have been excluded from the reference sample. Sample groups and the critical values are given for the confidence levels separately.

Earthquake	Coordinate of test point	Study period	Periods of high geomagnetic activities	f	Critical values		Sample pairs	
					99%	95%	99%	95%
Haiti	.17. $5°N$, $75°W$	29 Nov-12 Jan	–	32	2.738	2.037	5, 12	12
Drake Passage	.57. $5°S$, $65°W$	4 Dec-17 Jan	–	32	2.738	2.037	6, 7	6
Chile	$35°S$, $75°W$	14 Jan-27 Feb	20 Jan, 2,15,16,17 Feb	30	2.750	2.042	–	–
Indonesia	$5°S$, $100°E$	20 Jan- 5 marc	20 Jan, 2,15,16,17 Feb	27	2.771	2.052	–	–
Turkey	$40°N$, $40°E$	23 Jan- 8 marc	2, 15, 16, 17 Feb	28	2.763	2.048	1, 3, 4, 6, 12	3, 4, 6
Honshu	.37. $5°N$, $140°E$	29 Jan-14 Marc	2, 15,16,17 Feb	28	2.763	2.048	10, 11, 12	10
Mexico	.32. $5°N$, $115°W$	19 Feb-4 Apr	–	32	2.738	2.037	8	–
Bio-Bio	.37. $5°S$, $75°W$	31 May-14 July	31 May- 1, 4,29, 30 June- 14 July	28	2.763	2.048	9	8
Ecuador	.2. $5°S$, $75°W$	28 July-12 Aug	29, 30 June- 14, 15, 27, 28 July- 3, 4, 5 Aug	26	2.779	2.056	8, 9	8, 9
New Zealand	.42. $5°S$, $170°E$	21 July- 3Sep	27, 28 July-3, 4, 5, 24, 25 Aug	27	2.771	2.052	–	3
Kerman	.27. $5°N$, $60°E$	6 Nov-20 Dec	11, 12, 27 Nov	29	2.756	2.045	1	–
Bonin	.27. $5°N$, $145°E$	7 Nov- 21 Dec	11, 12, 27 Nov	29	2.756	2.045	–	–

Table 3
The Haiti earthquake, the t-statistic values and the time periods of seismo-ionospheric anomalies. Time intervals are in UT.

Sample group	Days	0-2	2-4	4-6	6-8	8-10	10-12	12-14	14-16	16-18	18-20	20-22	22-24
1	29 Dec-1 Jan	3.32 ††	1.18	0.51	0.49	0.54	0.65	1.75	1.66	1.80	2.62 †	1.29	0.93
2	30 Dec-2 Jan	4.57 ††	1.27	1.23	0.23	0.49	1.56	2.68 †	2.09 †	2.55 †	3.28 ††	1.77	0.93
3	31 Dec-3 Jan	4.57 ††	0.86	0.60	0.70	1.77	2.66 †	3.09 ††	2.01	2.60 †	2.53 †	2.30 †	0.96
4	1-4 Jan	3.69 ††	0.26	0.29	0.24	1.16	2.58 †	3.18 ††	1.98	1.63	1.99	2.39 †	0.59
5	**2-5 Jan**	3.63 ††	0.26	0.16	0.77	1.11	2.31 †	3.13 ††	1.98	1.18	1.00	1.73	0.38
6	3-6 Jan	2.77 ††	0.72	0.80	0.83	0.81	2.31 †	2.73 ††	1.58	0.23	0.52	2.82 ††	1.21
7	4-7 Jan	1.97	0.01	0.45	0.62	0.52	1.93	2.82 ††	1.80	0.67	1.23	3.10 ††	1.55
8	5-8 Jan	2.36 †	1.52	1.67	0.72	1.12	2.53 †	2.24 †	1.58	1.16	1.33	2.04	1.22
9	6-9 Jan	1.54	0.53	1.62	0.01	0.35	0.66	1.61	1.62	1.08	2.43 †	2.12	1.04
10	7-10 Jan	2.35 †	2.58 †	4.10 ††	1.52	0.67	0.93	1.15	1.15	0.92	1.91	0.46	0.96
11	8-11 Jan	0.61	0.06	1.35	0.55	1.36	1.73	1.26	0.24	1.79	0.45	3.04 ††	3.23 ††
12	**9-12 Jan**	0.21	1.93	0.03	2.83 ††	2.56 †	2.94 ††	1.63	0.50	0.92	0.97	3.74 ††	3.98 ††

Table 4
The contribution of the daily TEC anomalies and time periods of significant TEC changes.

	0-2 (UT)	2-4 (UT)	4-6 (UT)	6-8 (UT)	8-10(UT)	10-12(UT)	12-14(UT)	14-16(UT)	16-18(UT)	18-20(UT)	20-22(UT)	22-24(UT)
9-Jan	1.979167	13.80471	5.333333	**17.48252**	**21.37746**	**22.73782**	7.142857	31.17932	12.94574	40.87933	**3.121248**	**0.324675**
10-Jan	42.60417	23.23232	45.33333	**19.23077**	**20.6619**	**15.54524**	11.49068	0.323102	12.63566	4.396632	**23.88956**	**25.64935**
11-Jan	54.27083	35.69024	43.55556	**24.82517**	**32.11091**	**45.93968**	70.49689	65.75121	66.12403	27.87652	**48.19928**	**51.62338**
12-Jan	1.145833	27.27273	5.777778	**38.46154**	**25.84973**	**15.77726**	10.86957	2.746365	8.294574	26.84752	**24.78992**	**22.4026**

are reported in other researches is not a straight forward process. Nevertheless, among the 12 earthquakes of this study, Haiti is a highly cited one whose anomaly has been confirmed by many researches. Therefore, we have also tried to compare ours to the existing results for this earthquake: By using the global ionospheric maps, Liu et al. (2011a,b) reported on remarkable changes in TEC one day before the Haiti earthquake. Such anomalies were observed at the vicinity of the earthquake epicenter and its geomagnetic conjugate region (Liu et al., 2011a). These anomalies were later confirmed in (Akhoondzadeh and Saradjian, 2011; Sarkar et al., 2012; Singh et al., 2010; Yao et al., 2012b). Seismo-ionospheric changes derived from the analysis of the sample pairs in this study, i.e. the reference and the 12^{th} target sample which starts from January 9 and ends at January 12; are also compatible with such results. Tables 3 and 4 report on the obtained results. Table 3 reports on the t-statistic values and the time periods of seismo-ionospheric anomalies. Table 4 gives the contribution of the daily TEC anomalies at the test point of this earthquake during the time period of the 12th target sample. The time periods in which significant TEC changes are observed, have been given in bold. Based on these results, significant TEC changes are seen at 6–12 UT and 20–24 UT. Moreover during this period of time, the contribution of TEC changes is higher in the January 11.

The effective precursor manifestation zone which we have derived from the analysis of TEC data using the T2-Hotelling test also conforms to the similar area which is reported in (Liu et al., 2011a) Fig. 3 illustrates this zone based on the results of the current study. Similar results as reported in Liu et al. (2011a,b) is reproduced in Fig. 4 for further comparisons.

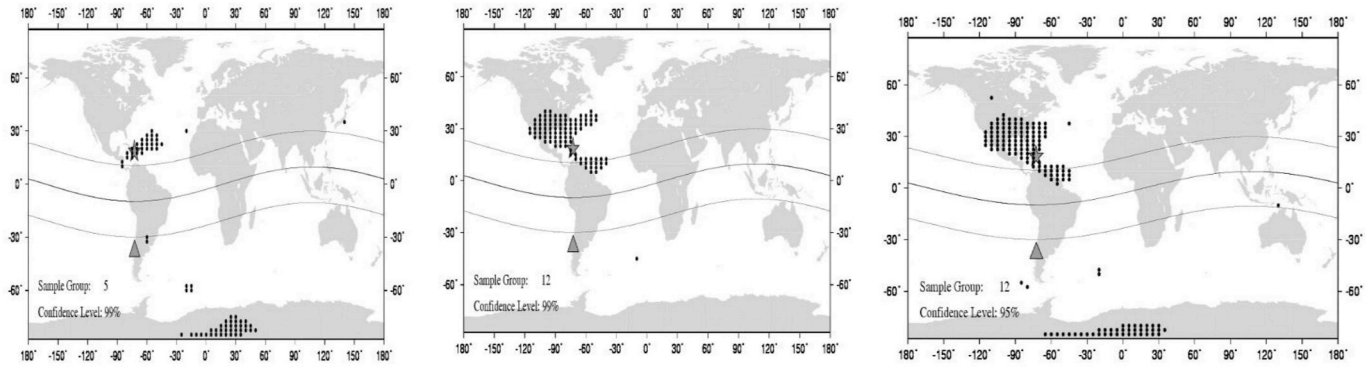

(1) (2) (3)

Fig. 3. The spatial distribution of seismo-ionospheric anomalies for the Haiti earthquake.

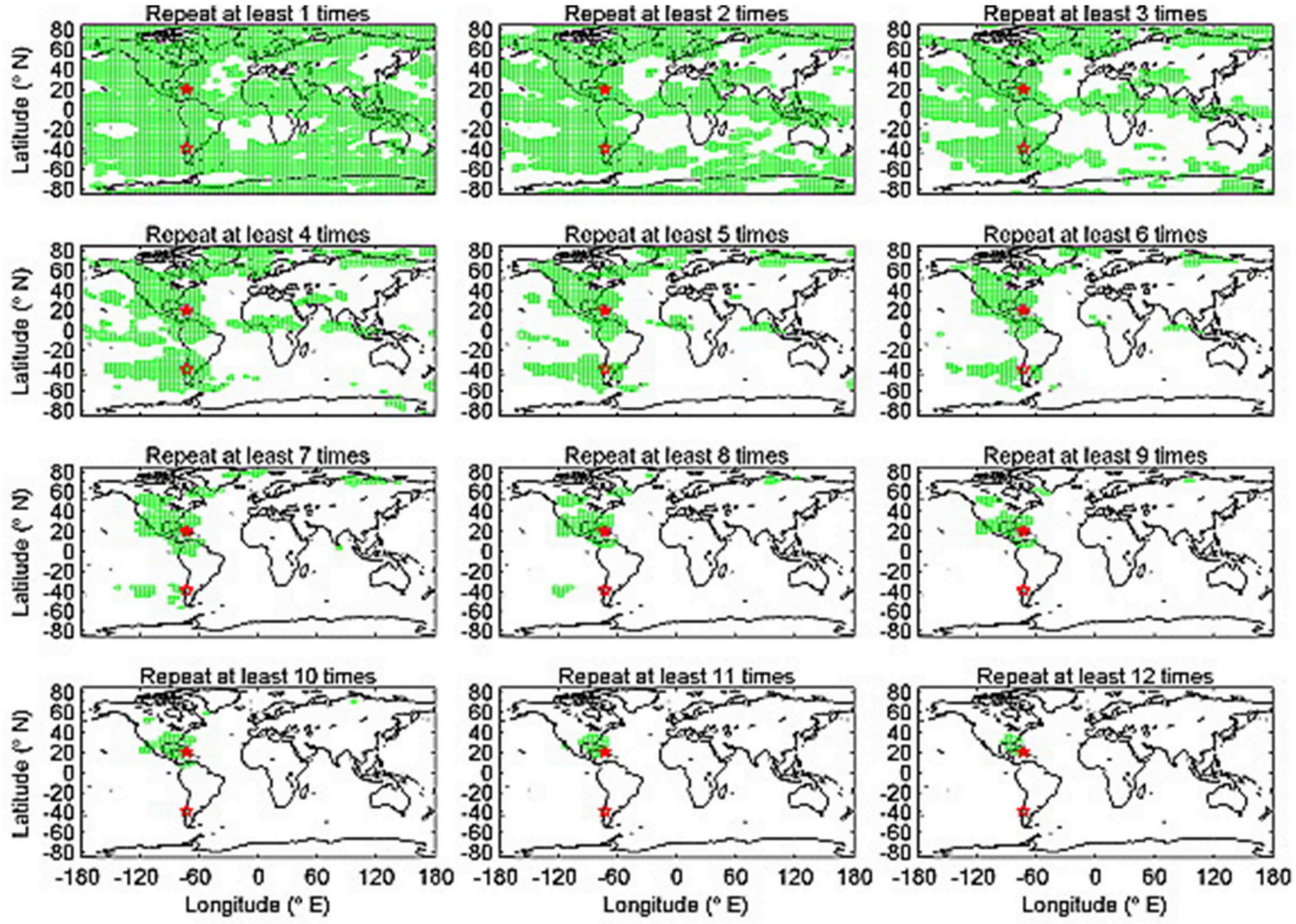

Fig. 4. The effective precursor manifestation zone for the Haiti earthquake (Liu et al., 2011a). Locations of the 30 day extreme enhancement (maximum) repeatedly appear at various time points on the local day of 11 January 2010 in Haiti. The number of the repeat time point is noted on top of each panel. The solid and open start symbols denote the epicenter and its conjugate point.

4.1. Some remarks on the other earthquakes

For 75% of the studied earthquakes, proposed method confirms the seismo-ionospheric anomalies that have been already reported in the other researches. The rest of the studied quakes conform to the assertion that seismo-ionospheric anomalies might not be clearly visible even for some large earthquakes (Le et al., 2015) For example, although significant disturbances have been discovered in the electric and geomagnetic fields as well as the electron density in ionosphere in advance of the Chile earthquake (Ho et al., 2013; Liu et al., 2011b) Yao et al. (2012b) see no remarkable changes in the TEC data when the GIMs are used. On contrary to Yao et al. (2012b); He and Heki (2016) report on abnormal variation in TEC 20–40 min before this earthquake. Similar to Yao et al. (2012b); by using TEC data, we do not detect seismo-ionospheric anomaly for this earthquake.

5. Conclusions

Today, the TEC anomaly is used as a measure for detecting ionospheric changes associated with some of the large earthquakes. Since 1970, many researchers have reported on seismo-ionospheric anomalies. Nevertheless, it is not still possible to certainly assign such variations to a specific earthquake. This is because; ionosphere by itself has significant variations from one day to another (Afraimovich et al., 2004; Le et al., 2013, 2015; Masci and Thomas, 2014; Masci et al., 2015; Thomas et al., 2012). Albeit it is still difficult to assign the observed changes to a certain quake, characteristics such as the frequency of the observed anomalies, their position as well as the corresponding time period are considered as the features that are frequently seen when ionospheric changes are analyzed before a large earthquake. This paper applies the T2-Hotelling test for analyzing the TEC variations and their association with large earthquakes. Detected anomalies are related to a certain seismic event if and only if they are associated with the characteristics mentioned above. Earthquake is a seismic geophysical phenomenon including irregular, nonlinear and complex processes and that's why there is no simple approach to predict its parameters. Simplifying the analysis of such a process is obviously inevitable specially when a single parameter (the TEC variation in this study for example) is used for this purpose. Although the requirements and assumptions in the proposed method limits the sample size of this research to 12 earthquakes, they are definitely supportive in this respect. For every earthquake, the proposed method is applied to the entire globe. As the result using the proposed method, it is possible to explore both the temporal and the spatial variations in TEC in global scale. For 75% of the earthquakes in this study, proposed method confirms the seismo-ionospheric anomalies have been already reported in the other researches. The rest of the studied quakes confirm the assertion that seismo-ionospheric anomalies might not be clearly visible even for some of the large earthquakes.

Appendix B. Supplementary data

Supplementary data to this article can be found online at https://doi.org/10.1016/j.jastp.2019.01.010.

Appendix A

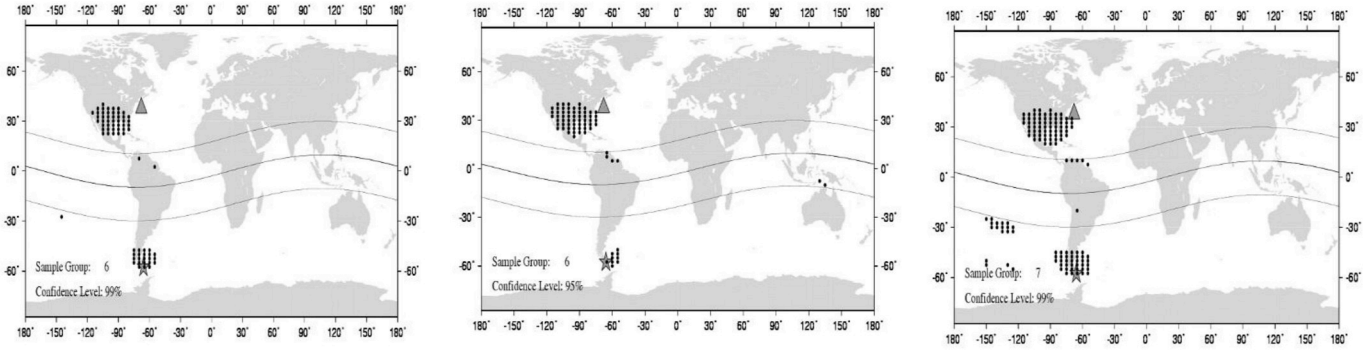

Fig. A1. The spatial distribution of seismo-ionospheric anomalies for the Drake Passage earthquake.

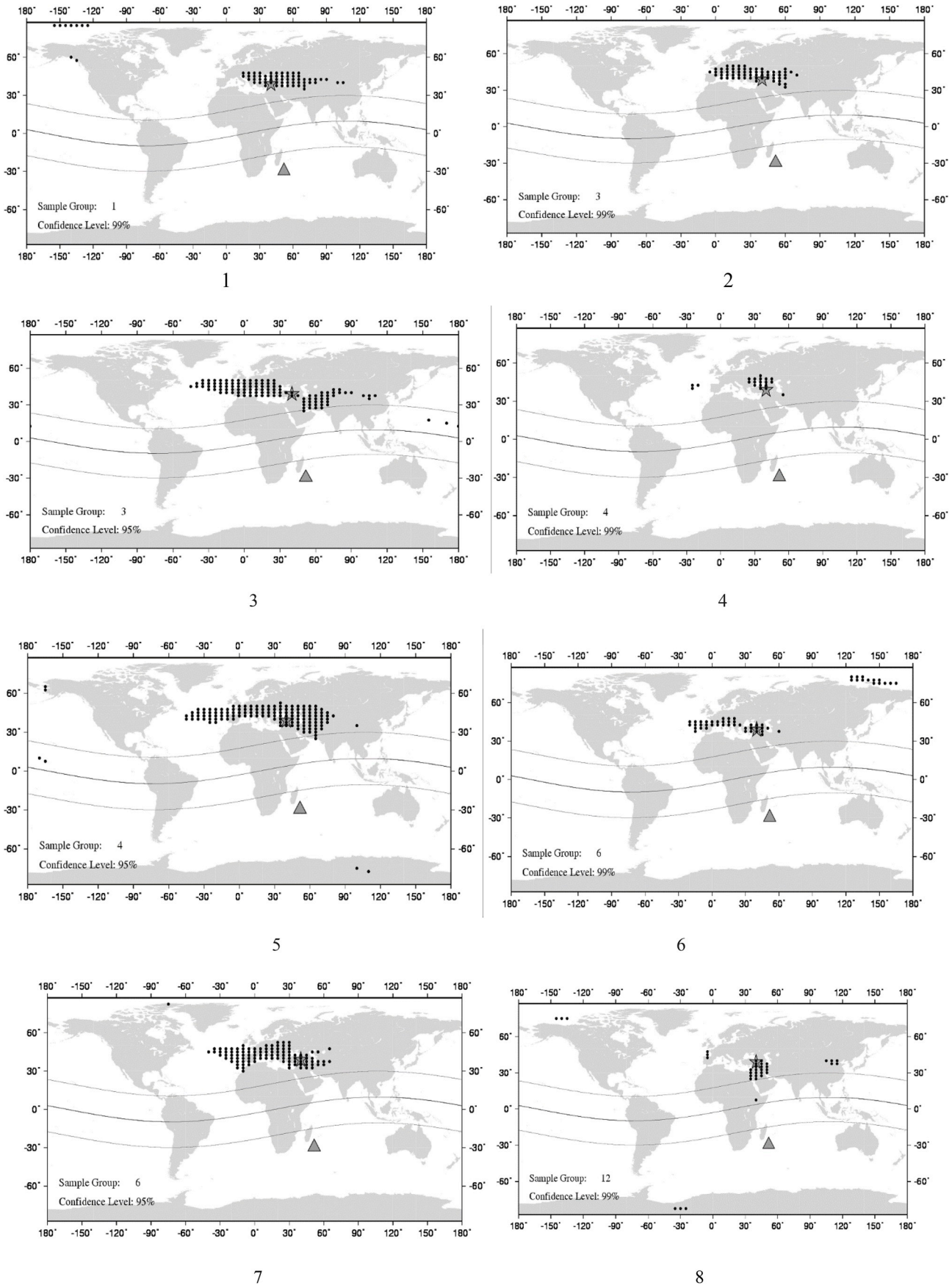

Fig. A2. The spatial distribution of seismo-ionospheric anomalies for the Turkey earthquake.

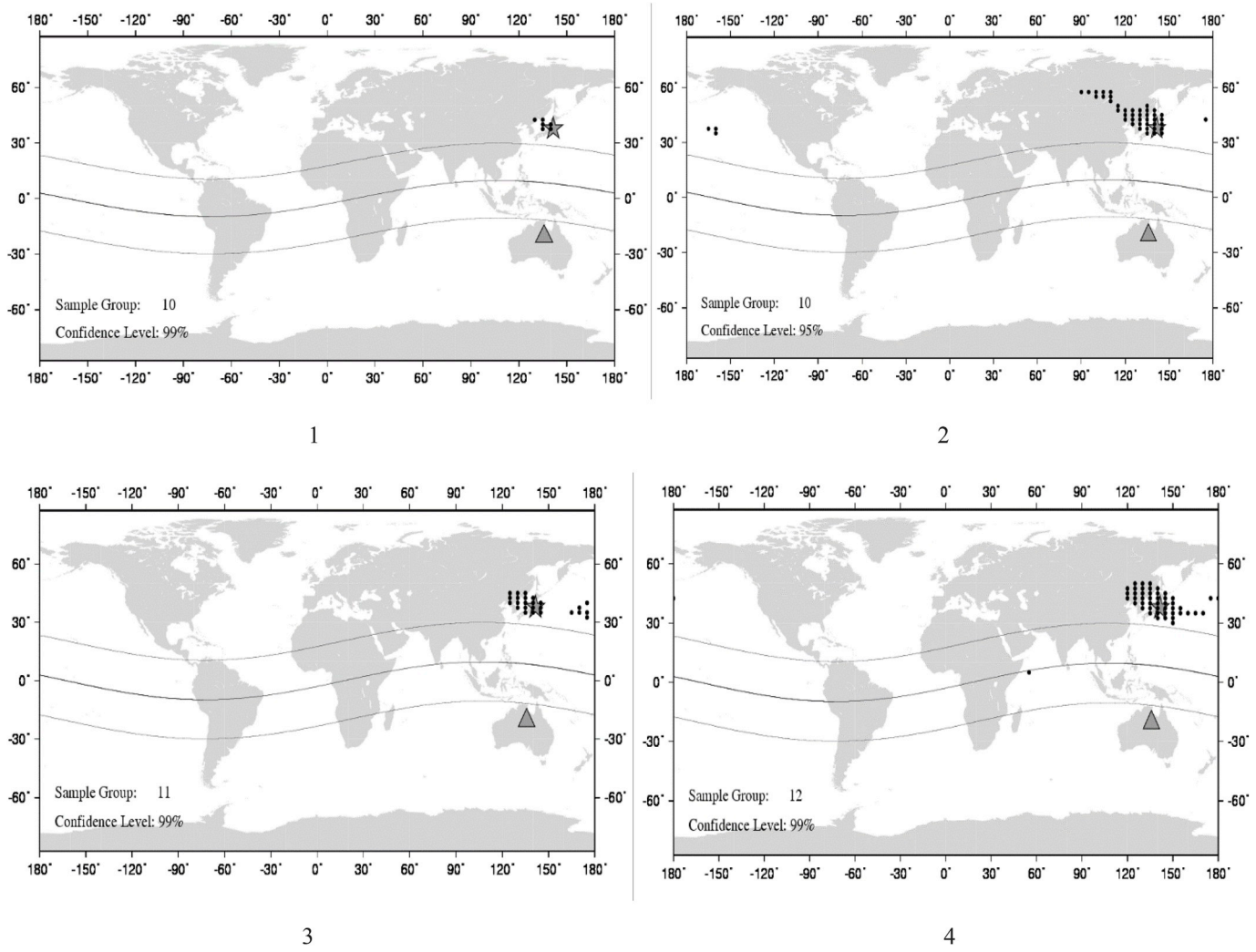

Fig. A3. The spatial distribution of seismo-ionospheric anomalies for the Honshu earthquake.

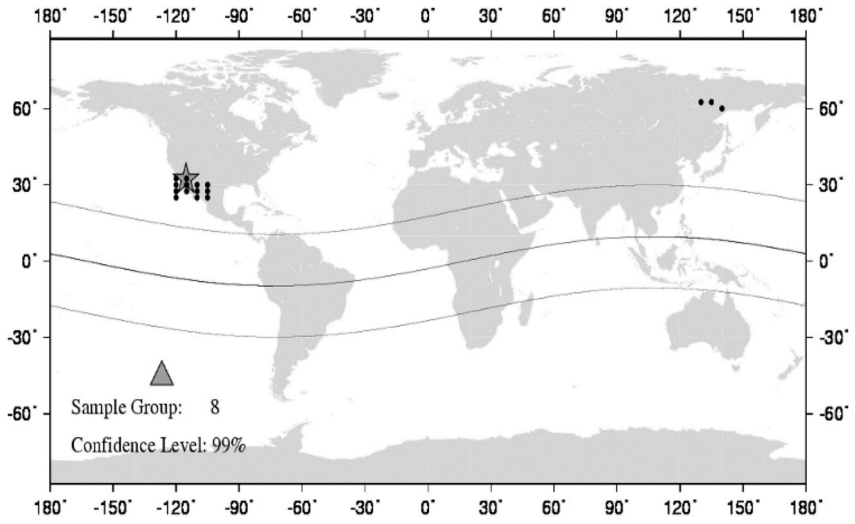

Fig. A4. The spatial distribution of seismo-ionospheric anomalies for the Mexico earthquake

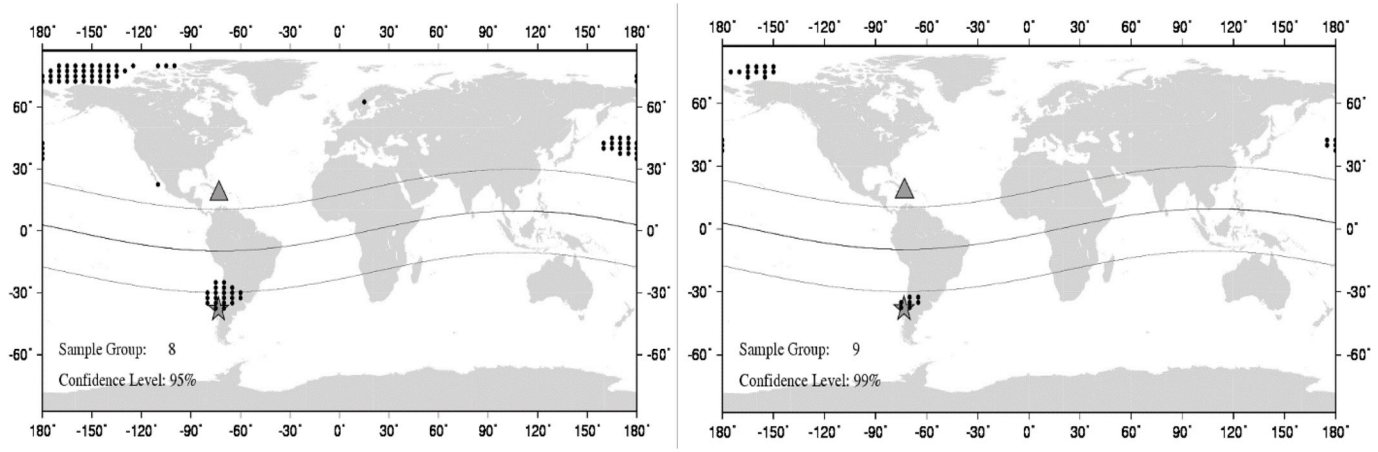

Fig. A5. The spatial distribution of seismo-ionospheric anomalies for the Bio-Bio earthquake.

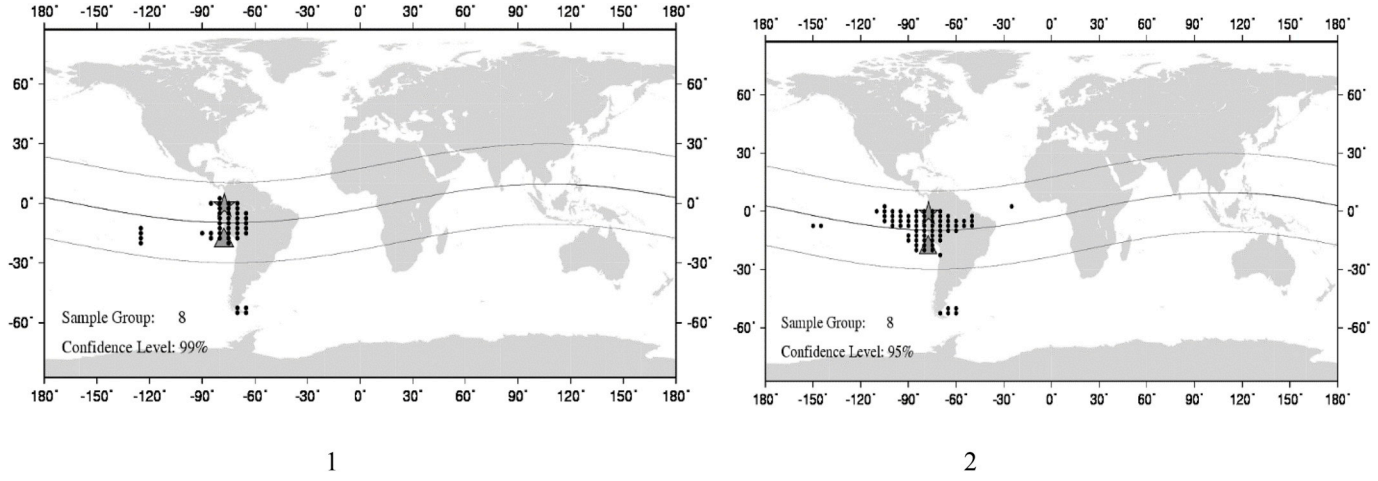

Fig. A6. The spatial distribution of seismo-ionospheric anomalies for the Ecuador earthquake.

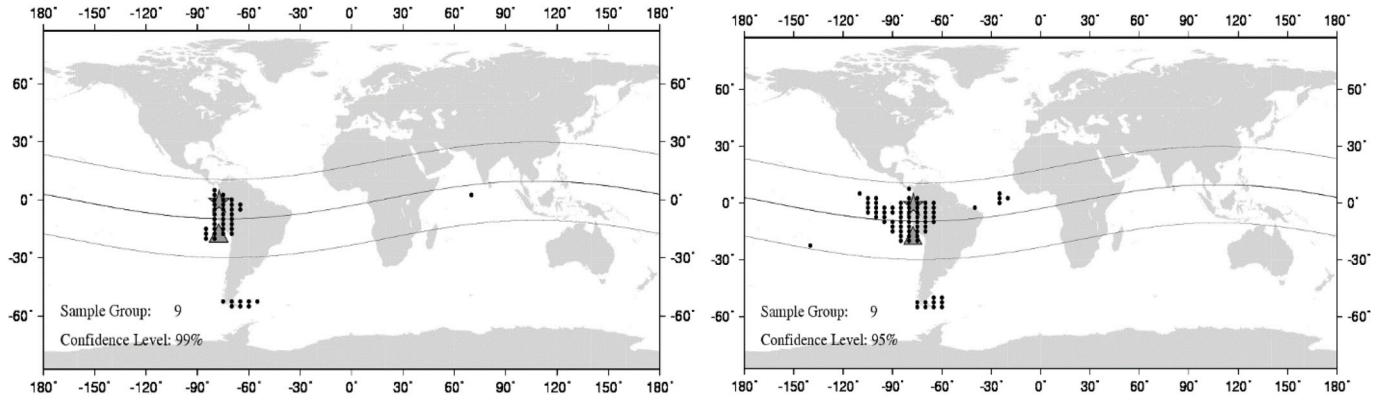

Fig. A7. The spatial distribution of seismo-ionospheric anomalies for the New Zealand earthquake.

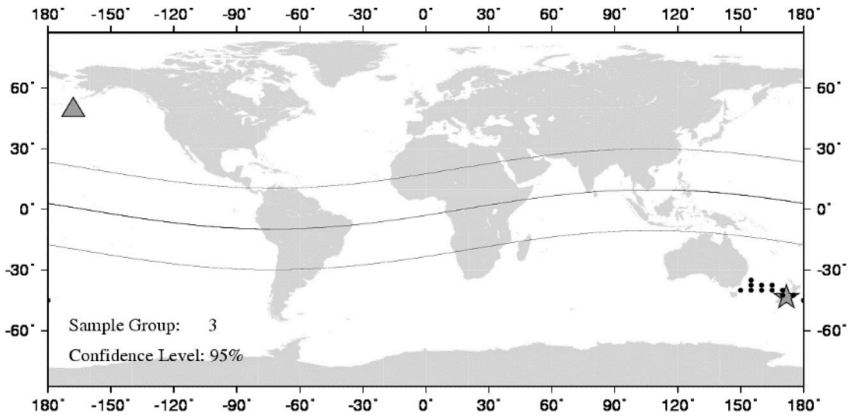

Fig. A8. The spatial distribution of seismo-ionospheric anomalies for the Kerman earthquake.

Table. A1
The Drake Passage earthquake, the t-statistic values and the time periods of seismo-ionospheric anomalies. Time intervals are in UT.

Sample group	Days	0-2	2-4	4-6	6-8	8-10	10-12	12-14	14-16	16-18	18-20	20-22	22-24
1	3-6 Jan	0.623	1.821	0.265	0.269	1.673	1.464	1.400	1.143	0.485	1.090	2.125 †	0.225
2	4-7 Jan	0.052	2.391 †	1.049	0.302	1.537	0.081	1.166	1.457	0.271	0.636	2.302 †	0.496
3	5-8 Jan	0.713	2.612 †	1.145	0.033	1.324	0.022	1.279	1.535	0.448	0.059	1.493	0.923
4	6-9 Jan	1.439	1.255	0.101	1.145	0.739	0.918	0.327	1.359	0.153	0.301	1.007	1.440
5	7-10 Jan	1.884	0.893	0.178	1.746	0.279	1.477	1.062	0.375	1.139	0.355	0.477	2.672†
6	**8-11 Jan**	3.412 ††	0.366	1.331	3.238 ††	0.893	1.372	2.213 †	0.689	1.568	0.604	2.076†	3.671 ††
7	**9-12 Jan**	5.662 ††	2.974††	2.361 †	4.070 ††	1.096	1.833	2.265 †	0.942	1.097	0.316	1.684	3.555 ††
8	10-13 Jan	6.354††	3.436 ††	2.706 †	4.070 ††	1.196	1.733	1.762	0.218	0.902	0.401	0.927	2.679 †
9	11-14 Jan	6.44 1††	3.685 ††	2.020	2.607 †	0.828	1.693	0.820	0.696	0.376	0.274	0.198	1.206
10	12-15 Jan	6.006 ††	4.399 ††	0.376	0.939	0.252	1.495	0.509	1.785	1.102	0.354	1.745	0.155
11	13-16 Jan	5.631 ††	2.680 †	0.806	0.516	1.169	1.688	2.141 †	1.699	1.875	1.067	1.886	0.249
12	14-17 Jan	5.631 ††	2.812 ††	1.549	1.805	2.229 †	1.708	2.533 †	1.255	2.434 †	1.110	2.431 †	0.290

Table. A2
The Chile earthquake, the t-statistic values and the time periods of seismo-ionospheric anomalies. Time intervals are in UT.

Sample group	Days	0–2	2–4	4–6	6–8	8–10	10–12	12–14	14–16	16–18	18–20	20–22	22–24
1	13–16 Feb	1.141	2.786††	3.106††	3.199††	3.128††	2.396†	0.417	0.928	2.727†	1.074	0.417	0.405
2	14–17 Feb	1.213	2.666†	2.357†	2.348†	2.325†	1.134	0.759	0.681	2.628†	1.449	1.014	0.822
3	15–18 Feb	1.799	3.616††	2.812††	2.536†	2.370†	0.488	1.054	0.626	2.438†	1.822	1.203	1.093
4	16–19 Feb	1.454	2.469†	1.981	1.522	1.585	0.645	1.574	0.147	1.486	2.026	1.371	1.068
5	17–20 Feb	0.468	0.870	0.937	0.288	0.853	1.076	1.878	0.203	0.824	2.167†	2.685†	1.793
6	18–21 Feb	0.101	0.267	0.590	0.109	0.767	0.895	2.124†	0.258	0.685	2.188†	3.463††	2.371†
7	19–22 Feb	0.404	0.719	0.126	0.116	0.704	0.895	2.211†	0.333	0.463	1.512	3.716††	2.840††
8	20–23 Feb	0.531	0.036	0.453	0.310	1.134	0.552	2.143†	0.515	1.134	1.450	3.242††	2.292†
9	21–24 Feb	0.173	0.497	0.037	0.025	0.997	0.355	1.868	0.515	1.134	1.048	2.667†	2.239†
10	22–25 Feb	0.722	0.695	0.226	0.371	0.192	0.873	1.836	0.533	1.280	1.239	2.503†	1.875
11	23–26 Feb	0.675	0.695	0.381	1.090	0.372	0.798	1.967	0.665	0.837	1.070	1.947	1.218
12	24–27 Feb	0.267	1.429	1.456	2.565†	1.447	1.895	2.760††	1.066	0.015	1.100	2.011	1.093

Table. A3
The Indonesia earthquake, the t-statistic values and the time periods of seismo-ionospheric anomalies. Time intervals are in UT.

Sample group	Days	0–2	2–4	4–6	6–8	8–10	10–12	12–14	14–16	16–18	18–20	20–22	22–24
1	19–22 Feb	1.344	1.228	3.428††	2.857††	3.259††	3.171††	2.354†	2.957††	2.678†	2.679†	2.056†	1.931
2	20–23 Feb	1.376	1.289	3.070††	2.528†	2.777††	2.321†	1.764	2.063†	1.860	2.176†	1.855	1.749
3	21–24 Feb	1.570	1.841	3.378††	2.670†	2.738†	2.553†	1.867	2.557†	2.658†	2.779††	2.012	2.112†
4	22–25 Feb	2.154†	2.675†	3.673††	2.690†	2.288†	1.904	1.457	2.033	1.719	1.570	1.722	2.547†
5	23–26 Feb	3.043††	3.003††	3.459††	2.716†	2.199†	1.644	0.707	1.058	0.902	1.473	1.699	2.732†
6	24–27 Feb	3.470††	3.217††	4.029††	2.946††	2.511†	2.115†	0.478	1.087	1.175	1.135	0.947	2.093†
7	25–28 Feb	2.784††	3.034††	4.175††	2.657†	1.925	1.226	0.040	0.450	0.410	0.279	0.807	1.943
8	26 Feb-1 Mar	2.649†	3.202††	4.476††	2.603†	1.937	1.393	0.140	0.070	0.410	0.934	0.851	1.641
9	27 Feb-2 Mar	2.179†	2.816††	4.532††	2.564†	1.926	1.657	0.054	0.023	0.767	1.073	0.563	1.113
10	28 Feb-3 Mar	1.872	2.576†	4.553††	2.646†	2.290†	1.738	0.243	0.125	1.168	1.979	0.875	1.426
11	1–4 Mar	2.232†	2.629†	4.331††	2.639†	3.059††	2.838††	0.441	0.031	1.555	3.102††	0.682	1.089
12	2–5 Mar	1.994	2.270†	3.920††	2.584†	3.166††	2.963††	0.521	0.249	1.304	2.497†	0.408	1.338

Table. A4
The Turkey earthquake, the t-statistic values and the time periods of seismo-ionospheric anomalies. Time intervals are in UT.

Sample group	Days	0-2	2-4	4-6	6-8	8-10	10-12	12-14	14-16	16-18	18-20	20-22	22-24
1	**22-25 Feb**	4.631 ††	4.938 ††	6.554 ††	5.375 ††	3.692 ††	2.636 †	1.976	1.957	2.829 ††	4.442 ††	4.366 ††	3.317 ††
2	23-26 Feb	4.446 ††	4.652 ††	5.429 ††	4.740 ††	3.969 ††	3.408 ††	2.288 †	1.336	2.225 †	3.616 ††	3.120 ††	2.496 †
3	**24-27 Feb**	3.722 ††	3.924 ††	4.776 ††	4.658 ††	3.969 ††	3.680 ††	2.081 †	1.834	2.427 †	4.001 ††	3.825 ††	2.855 ††
4	**25-28 Feb**	3.510 ††	3.338 ††	4.098 ††	4.207 ††	3.575 ††	3.630 ††	1.661	1.660	1.533	2.784 ††	3.224 ††	1.708
5	26 Feb-1 Mar	2.576 †	2.200 †	3.351 ††	3.658 ††	3.302 ††	2.895 ††	1.419	1.755	2.076 †	3.012 ††	4.093 ††	2.361 †
6	**27 Feb-2 Mar**	3.347 ††	2.913 ††	3.734 ††	3.620 ††	3.206 ††	2.445 †	0.780	2.224 †	3.134 ††	3.378 ††	4.928 ††	2.432 †
7	28 Feb- 3 Mar	3.617 ††	3.101 ††	3.548 ††	3.549 ††	3.992 ††	2.162 †	1.205	2.263 †	3.104 ††	2.657 ††	4.016 ††	1.882
8	1-4 Mar	3.481 ††	2.826 ††	2.902 ††	3.338 ††	4.855 ††	1.648	1.051	2.488 †	4.018 ††	3.264 ††	3.775 ††	1.844
9	2-5 Mar	3.519 ††	3.368 ††	2.969 ††	3.213 ††	4.365 ††	1.681	1.378	2.527 †	3.730 ††	2.491 †	3.282 ††	1.058
10	3-6 Mar	2.841 ††	2.533 †	2.586 †	2.452 †	3.393 ††	1.424	1.796	2.812 ††	3.674 ††	2.294 †	2.766 ††	1.025
11	4-7 Mar	2.251 †	2.045	2.412 †	2.041	2.845 †	1.917	1.346	3.102 ††	4.222 ††	2.615 †	3.334 ††	1.059
12	**5-8 Mar**	2.157 †	2.007	2.896 ††	1.984	1.925	2.084 †	2.010	2.972 ††	3.509 ††	2.401 †	3.772 ††	1.477

Table. A5
The Honshu earthquake, the t-statistic values and the time periods of seismo-ionospheric anomalies. Time intervals are in UT.

Sample group	Days	0-2	2-4	4-6	6-8	8-10	10-12	12-14	14-16	16-18	18-20	20-22	22-24
1	28 Feb-3 Mar	0.015	0.413	0.162	0.194	1.339	1.078	0.603	0.103	1.191	0.188	0.090	1.206
2	1-4 Mar	0.454	0.899	0.088	0.765	2.530 †	1.478	0.897	0.466	1.746	0.710	0.171	1.435
3	2-5 Mar	1.199	1.366	0.573	1.251	2.781	1.771	0.653	0.950	2.145 †	1.084	0.049	1.248
4	3-6 Mar	0.845	1.464	1.058	1.655	3.165	1.664	0.032	0.575	1.706	0.793	0.192	0.925
5	4-7 Mar	0.390	1.767	2.756 †	2.305 †	3.464	1.912	0.114	0.496	1.580	0.699	0.273	0.925
6	5-8 Mar	0.252	1.410	2.713 †	1.513	2.658 †	1.764	0.195	0.418	1.373	0.653	0.639	0.573
7	6-9 Mar	0.529	0.916	2.733 †	1.708	2.613 †	2.070 †	0.476	0.495	1.719	0.786	1.061	0.880
8	7-10 Mar	0.388	0.978	2.435 †	2.369 †	2.682 †	3.039 ††	1.973	1.916	2.859 ††	2.076 †	1.982	1.736
9	8-11 Mar	0.289	0.918	2.113 †	2.325 †	2.760 †	3.481 ††	2.319 †	2.481 †	3.589 ††	2.845 ††	2.447 †	2.176 †
10	**9-12 Mar**	0.543	1.401	3.428 ††	3.911 ††	3.748 ††	5.214 ††	3.561 ††	3.908 ††	5.123 ††	4.521 ††	3.551 ††	3.061 ††
11	**10-13 Mar**	1.471	2.552 †	4.409 ††	4.803 ††	4.228 ††	6.527 ††	4.729 ††	4.763 ††	5.758 ††	5.467 ††	4.154 ††	3.625 ††
12	**11-14 Mar**	2.477 †	2.721 †	5.187 ††	5.198 ††	4.684 ††	7.004 ††	5.169 ††	5.356 ††	6.194 ††	6.248 ††	4.878 ††	4.225 ††

Table. A6
The Mexico earthquake, the t-statistic values and the time periods of seismo-ionospheric anomalies. Time intervals are in UT.

Sample group	Days	0-2	2-4	4-6	6-8	8-10	10-12	12-14	14-16	16-18	18-20	20-22	22-24
1	21-24 Marc	2.212 †	1.489	0.320	1.665	1.794	0.873	1.775	1.051	1.325	1.341	2.292 †	1.676
2	22-25 Marc	2.579 †	1.982	0.378	1.329	1.299	0.555	1.301	1.520	1.914	2.261 †	2.944 ††	2.518 †
3	23-26 Marc	2.837 ††	2.176 †	1.580	0.064	0.136	0.522	0.131	2.531 †	3.323 ††	2.685 †	2.410 †	3.059 ††
4	24-27 Marc	3.925 ††	2.106 †	1.912	0.470	0.335	1.063	0.619	3.018 ††	3.079 ††	2.907 ††	2.888 ††	3.996 ††
5	25-28 Marc	4.699 ††	2.405 †	1.519	0.264	0.056	0.701	0.127	3.018 ††	3.283 ††	2.658 †	2.800 ††	4.518 ††
6	26-29 Marc	4.592 ††	1.902	0.796	0.173	0.501	0.137	0.335	2.782 ††	2.784 ††	1.491	2.044 †	3.551 ††
7	27-30 Marc	4.126 ††	2.179 †	0.248	1.160	1.641	0.998	1.795	1.758	1.416	0.767	2.753 ††	4.089 ††
8	**28-31 marc**	4.246 ††	1.983	0.500	1.641	2.572 †	1.897	3.082 ††	0.824	1.234	1.133	2.922 ††	3.933 ††
9	29 Marc-1 Apr	3.836 ††	2.030	0.281	0.999	1.955	1.118	2.411 †	0.754	0.104	0.952	1.994	2.619 †
10	30 Marc-2 Apr	3.401 ††	1.813	1.035	0.105	1.024	0.580	2.219 †	0.174	1.147	0.627	1.222	1.305
11	31 Marc-3 Apr	1.800	0.889	1.104	0.798	0.418	0.181	1.408	0.495	1.313	0.739	0.555	0.287
12	1-4 Apr	0.686	1.183	2.800 ††	1.951	0.865	1.313	0.221	1.210	1.778	0.183	0.704	1.018

Table. A7
The Bio-Bio earthquake, the t-statistic values and the time periods of seismo-ionospheric anomalies. Time intervals are in UT.

Sample group	Days	0-2	2-4	4-6	6-8	8-10	10-12	12-14	14-16	16-18	18-20	20-22	22-24
1	30 Jun-3 Jul	0.290	0.624	1.499	1.039	0.483	0.142	0.491	0.394	0.266	1.157	0.996	0.635
2	1-4 Jul	0.034	0.314	0.644	0.170	0.184	0.257	0.432	0.680	0.266	0.724	0.678	0.602
3	2-5 Jul	0.070	0.723	0.700	0.176	0.533	0.486	0.076	0.253	0.624	0.099	0.802	0.909
4	3-6 Jul	0.332	0.227	0.339	1.107	1.053	0.947	0.098	0.091	0.676	0.447	1.222	0.670
5	4-7 Jul	0.369	0.655	0.145	0.214	0.266	0.301	0.408	0.383	1.227	0.378	2.576 †	0.684
6	5-8 Jul	0.149	0.787	0.460	0.465	0.494	0.085	0.628	0.786	1.057	1.118	1.754	1.370
7	6-9 Jul	1.175	0.173	0.012	0.357	0.796	0.025	0.688	1.007	0.377	2.420 †	1.372	1.849
8	**7-10 Jul**	1.924	0.080	0.012	0.304	0.745	0.292	0.234	0.656	2.190 †	3.543 ††	0.783	1.990
9	**8-11 Jul**	2.082 †	0.562	0.384	0.333	0.221	0.688	0.127	0.022	3.089 ††	3.449 ††	0.614	0.879
10	9-12 Jul	2.157 †	1.050	1.033	1.416	0.438	1.313	0.428	1.198	2.037	3.479 ††	1.809	1.168
11	10-13 Jul	1.219	1.215	1.237	1.948	0.882	1.629	0.746	1.727	1.265	3.334 ††	2.641 †	2.445 †
12	11-14 Jul	0.244	0.381	0.649	1.161	0.079	0.906	0.017	1.357	1.366	0.917	1.446	3.820 ††

Table. A8
The Ecuador earthquake, the t-statistic values and the time periods of seismo-ionospheric anomalies. Time intervals are in UT.

Sample group	Days	0-2	2-4	4-6	6-8	8-10	10-12	12-14	14-16	16-18	18-20	20-22	22-24
1	29 Jul-1 Aug	2.467 †	0.827	1.507	3.228	1.597	0.902	0.448	0.938	2.913 ††	2.837 ††	4.139 ††	0.391
2	30 Jul- 2 Aug	1.455	1.092	1.586	2.837	1.597	1.234	0.680	1.194	2.785 ††	3.656 ††	4.051 ††	1.332
3	31 Jul-3 Aug	1.681	1.808	1.813	1.935	1.307	0.960	0.583	0.845	2.901 ††	3.992 ††	3.788 ††	1.773
4	1-4 Aug	1.389	2.497 †	3.319 ††	2.043	1.950	1.725	1.744	1.611	3.374 ††	2.480 †	2.042	1.519
5	2-5 Aug	1.652	3.305 ††	3.828 ††	2.345 †	2.471 †	2.258 †	2.561 †	2.394 †	4.018 ††	3.400 ††	2.428 †	3.846 ††
6	3-6 Aug	2.316 †	5.049 ††	4.884 ††	3.589 ††	4.070 ††	2.885 ††	2.877 ††	2.481 †	4.135 ††	2.879 ††	2.799 ††	4.393 ††
7	4-7 Aug	2.359 †	5.147 ††	5.824 ††	4.980 ††	5.381 ††	3.213 ††	4.742 ††	3.507 ††	4.375 ††	2.860 ††	2.829 ††	5.151 ††
8	**5-8 Aug**	2.712 †	5.608 ††	6.565 ††	5.307 ††	5.012 ††	2.620 †	4.019 ††	2.717 †	3.950 ††	4.402 ††	4.713 ††	4.670 ††
9	**6-9 Aug**	2.392 †	4.121 ††	5.354 ††	4.381 ††	3.725 ††	2.752 †	4.080 ††	3.050 ††	4.001 ††	4.478 ††	5.067 ††	4.799 ††
10	7-10 Aug	2.719 †	3.964 ††	5.930 ††	4.309 ††	3.171 ††	2.509 †	4.258 ††	3.605 ††	4.559 ††	5.208	5.164 ††	5.283 ††
11	8-11 Aug	3.275 ††	3.912 ††	5.825 ††	4.208 ††	2.988 ††	2.509 †	4.478 ††	3.780 ††	5.063 ††	6.140	5.870 ††	5.243 ††
12	9-12 Aug	3.427 ††	4.044 ††	5.459 ††	4.397 ††	3.225 ††	3.048 ††	5.020 ††	4.376 ††	5.845 ††	5.927	6.240 ††	7.168 ††

Table. A9
The New Zealand earthquake, the t-statistic values and the time periods of seismo-ionospheric anomalies. Time intervals are in UT.

Sample group	Days	0-2	2-4	4-6	6-8	8-10	10-12	12-14	14-16	16-18	18-20	20-22	22-24
1	20-23 Aug	0.631	1.066	0.405	0.246	0.646	0.334	0.740	0.428	1.413	2.665 †	3.250 ††	2.322 †
2	21-24 Aug	1.856	2.766 †	1.016	0.812	1.646	1.178	1.409	0.570	1.940	2.800 ††	4.434 ††	2.428 †
3	**22-25 Aug**	2.631 †	2.504 †	2.154 †	1.471	1.808	1.057	1.902	1.061	1.475	1.944	2.824 ††	1.783
4	23-26 Aug	2.121 †	2.235 †	2.573 †	1.877	2.230 †	1.463	2.522 †	1.381	1.618	1.715	2.419 †	1.322
5	24-27 Aug	1.257	1.885	2.779 ††	2.327 †	2.309 †	1.710	2.144 †	1.004	0.577	0.024	0.665	0.629
6	25-28 Aug	0.272	0.319	1.245	1.737	1.562	0.842	0.587	0.314	0.698	1.458	1.154	1.894
7	26-29 Aug	1.129	0.240	0.838	0.688	1.236	0.143	0.636	1.854	1.235	1.968	0.505	2.062 †
8	27-30 Aug	1.046	0.652	1.375	0.583	0.684	0.635	1.603	2.540 †	1.677	2.530 †	0.239	1.755
9	28-31 Aug	1.174	0.762	1.807	0.211	0.061	1.684	1.758	2.398	0.818	2.123 †	0.579	0.891
10	29 Aug-1 Sep	0.868	1.304	1.944	0.536	0.331	1.264	1.296	1.416	0.058	0.482	2.820 ††	0.174
11	30 Aug-2 Sep	0.157	0.018	0.091	0.395	1.366	0.184	0.071	0.149	0.912	1.273	3.209 ††	0.395
12	31 Aug-3 Sep	0.366	0.123	0.733	0.525	1.875	1.309	0.794	0.457	1.296	0.778	3.278 ††	0.340

Table. A10
The Kerman earthquake, the t-statistic values and the time periods of seismo-ionospheric anomalies. Time intervals are in UT.

Sample group	Days	0-2	2-4	4-6	6-8	8-10	10-12	12-14	14-16	16-18	18-20	20-22	22-24
1	**6-9 Dec**	2.960 ††	5.321 ††	1.283	0.023	2.837 ††	0.156	0.756	0.819	4.542 ††	1.818	2.249 †	0.088
2	7-10 Dec	2.776 ††	3.788 ††	1.242	0.023	2.148 †	0.468	0.401	0.934	4.293 ††	1.777	2.868 ††	0.271
3	8-11 Dec	2.274 †	2.117 †	0.252	1.067	0.901	0.890	0.210	1.029	3.848 ††	1.124	1.152	0.243
4	9-12 Dec	0.604	0.298	1.863	2.015	0.052	1.227	0.345	1.485	3.030 ††	0.034	0.357	0.949
5	10-13 Dec	0.970	2.808 ††	3.748 ††	2.918 ††	0.802	1.891	1.754	2.344 †	0.249	2.042	2.351 †	1.867
6	11-14 Dec	1.607	4.308 ††	4.886 ††	3.851 ††	1.925	2.701 †	2.571 †	2.889 ††	0.813	3.761 ††	4.737 ††	2.853 ††
7	12-15 Dec	2.310 †	6.823 ††	5.717 ††	4.386 ††	1.446	2.383 †	2.955 ††	3.925 ††	3.187 ††	5.982 ††	6.763 ††	3.782 ††
8	13-16 Dec	3.165 ††	11.773††	6.499 ††	5.253 ††	2.275 †	3.140 ††	4.131 ††	4.524 ††	6.470 ††	8.851 ††	11.351 ††	4.525 ††
9	14-17 Dec	2.940 ††	12.350 ††	6.225 ††	5.253 ††	2.826 ††	3.152 ††	3.593 ††	4.573 ††	6.682 ††	8.851 ††	12.204 ††	4.767 ††
10	15-18 Dec	3.698 ††	12.523 ††	6.327 ††	5.866 ††	3.125 ††	3.464 ††	4.241 ††	4.991 ††	7.833 ††	8.470 ††	12.352 ††	4.767 ††
11	16-19 Dec	3.754 ††	12.700 ††	6.823 ††	6.522 ††	4.099 ††	4.510 ††	5.645 ††	5.218 ††	7.931 ††	8.197 ††	11.615 ††	4.358 ††
12	17-20 Dec	3.646 ††	12.754 ††	7.089 ††	6.036 ††	4.144 ††	4.807 ††	6.885 ††	5.128 ††	7.437 ††	7.769 ††	10.857 ††	4.358 ††

Table. A11
The Bonin Island earthquake, the t-statistic values and the time periods of seismo-ionospheric anomalies. Time intervals are in UT.

Sample group	Days	0–2	2–4	4–6	6–8	8–10	10–12	12–14	14–16	16–18	18–20	20–22	22–24
1	7–10 Dec	1.283	0.969	0.971	0.513	0.562	1.673	0.918	0.098	1.904	0.702	1.125	2.624†
2	8–11 Dec	1.990	0.945	0.799	0.002	1.319	2.811††	2.137†	0.451	2.634†	1.302	1.601	3.074††
3	9–12 Dec	2.164†	1.055	0.807	0.138	1.689	3.918††	3.417††	1.513	3.446††	2.447†	1.331	4.285††
4	10–13 Dec	3.097††	0.138	0.631	1.150	2.527†	4.853††	4.654††	3.303††	4.230††	3.491††	2.016	5.449††
5	11–14 Dec	4.074††	1.205	1.912	1.781	2.314†	4.789††	5.038††	3.812††	5.197††	4.110††	2.855††	5.523††
6	12–15 Dec	3.795††	1.462	2.116†	1.547	2.079†	4.241††	6.348††	5.764††	6.449††	5.670††	4.440††	6.766††
7	13–16 Dec	3.906††	1.900	2.687†	2.299†	2.841††	4.746††	8.059††	8.478††	8.749††	9.739††	8.167††	8.629††
8	14–17 Dec	4.136††	2.007	2.898††	3.180††	3.179††	4.725††	8.201††	8.345††	9.208††	9.820††	9.243††	8.947††
9	15–18 Dec	4.260††	2.140†	3.650††	4.359††	3.990††	5.257††	8.417††	8.570††	9.208††	10.165††	8.880††	9.233††
10	16–19 Dec	4.683††	2.849††	4.289††	5.902††	5.708††	6.989††	8.950††	8.258††	10.398††	11.268††	9.433††	9.644††
11	17–20 Dec	6.378††	4.306††	4.841††	6.231††	5.597††	7.032††	9.014††	8.841††	9.923††	12.119††	9.756††	9.991††
12	18–21 Dec	5.701††	3.634††	4.832††	5.545††	5.471††	6.879††	9.055††	8.891††	9.416††	11.836††	9.715††	10.330††

References

Afraimovich, E., Astafieva, E., Gokhberg, M., Lapshin, V., Permyakova, V., Steblov, G., Shalimov, S., 2004. Variations of the total electron content in the ionosphere from GPS data recorded during the Hector Mine earthquake of October 16, 1999, California. Russ. J. Earth Sci. 6 (5), 339–354.

Akhoondzadeh, M., 2011. Comparative Study of the Earthquake Precursors Obtained from Satellite Data. PhD thesis. University of Tehran, Surveying and Geomatics Engineering Department, Remote Sensing Division.

Akhoondzadeh, M., 2012. Anomalous TEC variations associated with the powerful Tohoku earthquake of 11 March 2011. Nat. Hazards Earth Syst. Sci. 12 (5), 1453–1462.

Akhoondzadeh, M., 2013a. An adaptive network-based Fuzzy inference system for the detection of thermal and TEC anomalies around the time of the varzeghan, Iran, (Mw = 6.4) earthquake of 11 august 2012. Adv. Space Res. 52 (5), 837–852.

Akhoondzadeh, M., 2013b. Genetic algorithm for TEC seismo-ionospheric anomalies detection around the time of the Solomon (Mw = 8.0) earthquake of 06 February 2013. Adv. Space Res. 52 (4), 581–590.

Akhoondzadeh, M., 2013c. A MLP neural network as an investigator of TEC time series to detect seismo-ionospheric anomalies. Adv. Space Res. 51 (11), 2048–2057.

Akhoondzadeh, M., 2013d. Support Vector Machines for TEC Seismo-Ionospheric Anomalies Detection. Annales Geophysicae, Copernicus GmbH.

Akhoondzadeh, M., 2013e. Support vector machines for TEC seismo-ionospheric anomalies detection. Ann. Geophys. 31 (2), 09927689.

Akhoondzadeh, M., 2014. Thermal and TEC anomalies detection using an intelligent

hybrid system around the time of the Saravan, Iran,(Mw= 7.7) earthquake of 16 April 2013. Adv. Space Res. 53 (4), 647–655.
Akhoondzadeh, M., Saradjian, M., 2011. TEC variations analysis concerning Haiti (January 12, 2010) and Samoa (September 29, 2009) earthquakes. Adv. Space Res. 47 (1), 94–104.
Alcay, S., 2016. Analysis of ionospheric tec variations response to the Mw 7.2 van earthquake. Acta Geodyn. Geomater. 13 (3), 257–262.
Calais, E., Minster, J.B., 1995. GPS detection of ionospheric perturbations following the January 17, 1994, Northridge earthquake. Geophys. Res. Lett. 22 (9), 1045–1048.
Davies, K., Baker, D.M., 1965. Ionospheric effects observed around the time of the Alaskan earthquake of March 28, 1964. J. Geophys. Res. 70 (9), 2251–2253.
Dobrovolsky, I., Zubkov, S., Miachkin, V., 1979. Estimation of the size of earthquake preparation zones. Pure Appl. Geophys. 117 (5), 1025–1044.
Freund, F., 2002. Charge generation and propagation in igneous rocks. J. Geodyn. 33 (4–5), 543–570.
Harrison, R.G., Aplin, K., Rycroft, M., 2010. Atmospheric electricity coupling between earthquake regions and the ionosphere. J. Atmos. Sol. Terr. Phys. 72 (5–6), 376–381.
Hayakawa, M., Molchanov, O.A., 2002. Seismo Electromagnetics: Lithosphere-Atmosphere-Ionosphere Coupling.
He, L., Heki, K., 2016. Three-dimensional distribution of ionospheric anomalies prior to three large earthquakes in Chile. Geophys. Res. Lett. 43 (14), 7287–7293.
Hirooka, S., Hattori, K., Nishihashi, M., Takeda, T., 2011. Neural network based tomographic approach to detect earthquake-related ionospheric anomalies. Nat. Hazards Earth Syst. Sci. 11 (8), 2341–2353.
Ho, Y.-Y., Jhuang, H.-K., Su, Y.-C., Liu, J.-Y., 2013. Seismo-ionospheric anomalies in total electron content of the GIM and electron density of DEMETER before the 27 February 2010 M8. 8 Chile earthquake. Adv. Space Res. 51 (12), 2309–2315.
Hotelling, H., 1992. The Generalization of Student's Ratio. Breakthroughs in Statistics. Springer, pp. 54–65.
Jyh-Woei, L., 2011. Use of principal component analysis in the identification of the spatial pattern of an ionospheric total electron content anomalies after China's May 12, 2008, M= 7.9 Wenchuan earthquake. Adv. Space Res. 47 (11), 1983–1989.
Le, H., Liu, J.-Y., Liu, L., 2011. A statistical analysis of ionospheric anomalies before 736 M6. 0+ earthquakes during 2002–2010. J. Geophys. Res.: Space Phys. 116, A02303. https://doi.org/10.1029/2010JA015781.".
Le, H., Liu, J., Zhao, B., Liu, L., 2015. Recent progress in ionospheric earthquake precursor study in China: a brief review. J. Asian Earth Sci. 114, 420–430.
Le, H., Liu, L., Liu, J.-Y., Zhao, B., Chen, Y., Wan, W., 2013. The ionospheric anomalies prior to the M9. 0 Tohoku-Oki earthquake. J. Asian Earth Sci. 62, 476–484.
Leonard, R.S., Barnes, R., 1965. Observation of ionospheric disturbances following the Alaska earthquake. J. Geophys. Res. 70 (5), 1250–1253.
Li, W., Guo, J., Yue, J., Shen, Y., Yang, Y., 2016. Total electron content anomalies associated with global VEI4+ volcanic eruptions during 2002–2015. J. Volcanol. Geoth. Res. 325, 98–109.
Liperovsky, V., Pokhotelov, O., Meister, C.-V., Liperovskaya, E., 2008. Physical models of coupling in the lithosphere-atmosphere-ionosphere system before earthquakes. Geomagn. Aeron. 48 (6), 795–806.
Liu, J.-Y., Chen, S.-W., Chen, Y.-C., Yen, H.-Y., Chang, C.-P., Chang, W.-Y., Tsai, L.-C., Chen, C.-H., Yang, W.-H., 2008. Seismo-ionospheric precursors of the 26 December 2006 M 7.0 pingtung earthquake doublet. Terr. Atmos. Ocean Sci. 19 (6).
Liu, J.-Y., Chen, Y., Chen, C.-H., Liu, C., Chen, C., Nishihashi, M., Li, J., Xia, Y., Oyama, K., Hattori, K., 2009. Seismoionospheric GPS total electron content anomalies observed before the 12 May 2008 Mw7. 9 Wenchuan earthquake. J. Geophys. Res.: Space Phys. 114 (A4).
Liu, J.-Y., Chen, Y., Chuo, Y., Chen, C.-S., 2006. A statistical investigation of pre-earthquake ionospheric anomaly. J. Geophys. Res.: Space Phys. 111 (A5).
Liu, J., Chen, Y., Chen, C., Hattori, K., 2010. Temporal and spatial precursors in the ionospheric global positioning system (GPS) total electron content observed before the 26 December 2004 M9. 3 Sumatra–Andaman Earthquake. J. Geophys. Res.: Space Phys. 115 (A9).
Liu, J., Chen, Y., Chuo, Y., Tsai, H., 2001. Variations of ionospheric total electron content during the Chi-Chi earthquake. Geophys. Res. Lett. 28 (7), 1383–1386.
Liu, J., Chen, Y., Pulinets, S., Tsai, Y., Chuo, Y., 2000. Seismo-ionospheric signatures prior to M≥ 6.0 Taiwan earthquakes. Geophys. Res. Lett. 27 (19), 3113–3116.
Liu, J., Le, H., Chen, Y., Chen, C., Liu, L., Wan, W., Su, Y., Sun, Y., Lin, C., Chen, M., 2011a. Observations and simulations of seismoionospheric GPS total electron content anomalies before the 12 January 2010 M7 Haiti earthquake. J. Geophys. Res.: Space Phys. 116 (A4).
Liu, J., Wan, W.X., Huang, J.P., Zhang, X.M., Zhao, S.F., Ouyang, X.Y., Zeren, Z.M., 2011b. Electron density perturbation before the 27 February 2010 Chile M8. 8 earthquake. Chin. J. Geophys. 54 (6), 737–746.
Liu, J.Y., Chuo, Y., Shan, S., Tsai, Y., Chen, Y., Pulinets, S., Yu, S., 2004. Pre-earthquake ionospheric anomalies registered by continuous GPS TEC measurements. Ann. Geophys. 22, 585–1593.
Lognonné, P., Artru, J., Garcia, R., Crespon, F., Ducic, V., Jeansou, E., Occhipinti, G., Helbert, J., Moreaux, G., Godet, P.-E., 2006. Ground-based GPS imaging of ionospheric post-seismic signal. Planet. Space Sci. 54 (5), 528–540.
Masci, F., Thomas, J., 2014. Comment on "Temporal and spatial precursors in ionospheric total electron content of the 16 October 1999 Mw 7.1 Hector Mine earthquake" by Su et al.(2013). J. Geophys. Res.: Space Phys. 119 (8), 6994–6997.
Masci, F., Thomas, J., Villani, F., Secan, J., Rivera, N., 2015. On the onset of ionospheric precursors 40 min before strong earthquakes. J. Geophys. Res.: Space Phys. 120 (2), 1383–1393.
Nenovski, P., Pezzopane, M., Ciraolo, L., Vellante, M., Villante, U., De Lauretis, M., 2015. Local changes in the total electron content immediately before the 2009 Abruzzo earthquake. Adv. Space Res. 55 (1), 243–258.
Oikonomou, C., H. Haralambous, B. Muslim "Investigation of ionospheric TEC precursors related to the M7. 8 Nepal and M8. 3 Chile earthquakes in 2015 based on spectral and statistical analysis." Nat. Hazards: 1-20.
Parrot, M., 2017. Electromagnetic Noise Due to Earthquakes. Handbook of Atmospheric Electrodynamics. CRC Press, pp. 105–126 1995.
Pertsev, N., Shalimov, S., 1996. The generation of atmospheric gravity waves in a seismically active region and their effect on the ionosphere. Geomagn. Aeron., Engl. Transl 36, 223–227.
Pulinets, S., Boyarchuk, K., 2004. Ionospheric Precursors of Earthquakes. Springer Science & Business Media.
Pulinets, S., Legen'Ka, A., Gaivoronskaya, T., Depuev, V.K., 2003. Main phenomenological features of ionospheric precursors of strong earthquakes. J. Atmos. Sol. Terr. Phys. 65 (16–18), 1337–1347.
Sarkar, S., Choudhary, S., Sonakia, A., Vishwakarma, A., Gwal, A., 2012. Ionospheric anomalies associated with the Haiti earthquake of 12 January 2010 observed by DEMETER satellite. Nat. Hazards Earth Syst. Sci. 12 (3), 671–678.
Shalimov, S., Gokhberg, M., 1998. Lithosphere–ionosphere coupling mechanism and its application to the earthquake in Iran on June 20, 1990. A review of ionospheric measurements and basic assumptions. Phys. Earth Planet. In. 105 (3–4), 211–218.
Singh, R.P., Mehdi, W., Sharma, M., 2010. Complementary nature of surface and atmospheric parameters associated with Haiti earthquake of 12 January 2010. Nat. Hazards Earth Syst. Sci. 10 (6).
Srivastava, M.S., Carter, E.M., 1983. An Introduction to Applied Multivariate Statistics. North-Holland.
Su, Y.-C., Liu, J.-Y., Chen, S.-P., Tsai, H.-F., Chen, M.-Q., 2013. Temporal and spatial precursors in ionospheric total electron content of the 16 October 1999 Mw7. 1 Hector Mine earthquake. J. Geophys. Res.: Space Phys. 118 (10), 6511–6517.
Thomas, J.N., Love, J.J., Komjathy, A., Verkhoglyadova, O.P., Butala, M., Rivera, N., 2012. On the reported ionospheric precursor of the 1999 Hector Mine, California earthquake. Geophys. Res. Lett. 39 (6).
Ulukavak, M., Yalcinkaya, M., 2016. Precursor analysis of ionospheric GPS-TEC variations before the 2010 M 7.2 Baja California earthquake. Geomatics, Nat. Hazards Risk 1–14.
Xu, T., Hu, Y., Wu, J., Wu, Z., Li, C., Xu, Z., Suo, Y., 2011. Anomalous enhancement of electric field derived from ionosonde data before the great Wenchuan earthquake. Adv. Space Res. 47 (6), 1001–1005.
Yao, Y., Chen, P., Wu, H., Zhang, S., Peng, W., 2012a. Analysis of ionospheric anomalies before the 2011 M w 9.0 Japan earthquake. Chin. Sci. Bull. 57 (5), 500–510.
Yao, Y., Chen, P., Zhang, S., Chen, J., Yan, F., Peng, W., 2012b. Analysis of pre-earthquake ionospheric anomalies before the global M= 7.0+ earthquakes in 2010. Nat. Hazards Earth Syst. Sci. 12 (3), 575–585.
Yiyan, Z., Yun, W., Xuejun, Q., Xunxie, Z., 2009. Ionospheric anomalies detected by ground-based GPS before the Mw7. 9 Wenchuan earthquake of May 12, 2008, China. J. Atmos. Sol. Terr. Phys. 71 (8), 959–966.
Zhao, B., Hao, Y., 2015. Ionospheric and geomagnetic disturbances caused by the 2008 Wenchuan earthquake: a revisit. J. Geophys. Res.: Space Phys. 120 (7), 5758–5777.
Zhao, B., Wang, M., Yu, T., Wan, W., Lei, J., Liu, L., Ning, B., 2008. Is an unusual large enhancement of ionospheric electron density linked with the 2008 great Wenchuan earthquake? J. Geophys. Res.: Space Phys. 113 (A11).
Zhu, F., Wu, Y., Zhou, Y., Gao, Y., 2013. Temporal and spatial distribution of GPS-TEC anomalies prior to the strong earthquakes. Astrophys. Space Sci. 345 (2), 239–246.
Zhu, F., Zhou, Y., Lin, J., Su, F., 2014. A statistical study on the temporal distribution of ionospheric TEC anomalies prior to M7. 0+ earthquakes during 2003–2012. Astrophys. Space Sci. 350 (2), 449–457.